



A hypervelocity star with a Magellanic origin

Denis Erkal¹,¹★ Douglas Boubert,² Alessia Gualandris,¹ N. Wyn Evans² and Fabio Antonini¹

¹Department of Physics, University of Surrey, Guildford GU2 7XH, UK

²Institute of Astronomy, University of Cambridge, Madingley Road, Cambridge CB3 0HA, UK

Accepted 2018 September 25. Received 2018 September 25; in original form 2018 April 26

ABSTRACT

Using proper motion measurements from *Gaia* Data Release 2, we probe the origin of 26 previously known hypervelocity stars (HVSs) around the Milky Way. We find that a significant fraction of these stars have a high probability of originating in the Milky Way Galaxy, but there is one obvious outlier. HVS3 is highly likely to be coming almost from the centre of the Large Magellanic Cloud (LMC). During its closest approach, $21.1^{+6.1}_{-4.6}$ Myr ago, it had a relative velocity of 870^{+69}_{-66} km s^{−1} with respect to the LMC. This large kick velocity is only consistent with the Hills mechanism, requiring a massive black hole near the centre of the LMC. This provides strong evidence that the LMC harbours a massive black hole of at least 4×10^3 – 10^4 M_⊙.

Key words: galaxies: hypervelocity stars – stars: kinematics and dynamics – galaxies: Magellanic Clouds.

1 INTRODUCTION

A hypervelocity star (HVS) is one whose velocity is sufficiently fast that it will escape the gravitational pull of the Milky Way (MW). The existence of this class of star was theorized by Hills (1988). If a binary star is disrupted by the massive black hole Sgr A*, then one of the stars could be ejected from the Galactic Centre at more than 1000 km s^{−1}. The first hypervelocity star (termed ‘HVS1’) was discovered by Brown et al. (2005) and interpreted as a vindication of the prediction. HVS1 is a 3 M_⊙ B star at a distance of 107 ± 15 kpc from the Sun and its extreme radial velocity 831.1 ± 5.7 km s^{−1} proves that it is unbound from the Galaxy (Brown, Geller & Kenyon 2014). The second hypervelocity star (HVS2) was discovered by Hirsch et al. (2005) and is rather different: the subdwarf O (sdO) star US 708 lies at only 8.5 ± 1.0 kpc and has a heliocentric velocity of 917 ± 7 km s^{−1} (Geier et al. 2015). The third hypervelocity star (HE 0437–5439 or HVS3) was discovered by Edelmann et al. (2005) and was similar to HVS1 rather than HVS2, being an 8 M_⊙ B star at a distance of 61 kpc (subsequent studies with improved spectroscopy found a slightly higher mass of ~ 9 M_⊙; Bonanos et al. 2008; Przybilla et al. 2008). Brown and collaborators subsequently conducted a targeted search for HVSs and identified a further 20 B HVSs in the halo of the MW that were similar to HVS1 (HVS4–HVS24 excluding HVS11; Brown et al. 2006, 2007, 2014). Further B-type HVS discoveries include HD 271791 (Heber et al. 2008a), HIP 60350 (Irrgang et al. 2010), and LAMOST-HVS1–LAMOST-HVS3 (Zheng et al. 2014; Huang et al. 2017).

There have been numerous claimed late-type HVSs within a few kiloparsec of the Sun (see Brown 2015, and references therein). However, these candidates are much less certain than the early-type B HVSs in the halo. B stars live short lives and thus their extreme radial velocities are corroborated by their need to travel that rapidly in order to survive the trip from regions of active star formation to their location in the halo. Late-type HVSs are often classed as HVSs based on large proper motions and there are several cases where their proper motions have proven erroneous. These candidates have recently been re-assessed by Boubert et al. (2018) in the light of *Gaia* Data Release 2 (DR2) and only one is truly unbound from the Galaxy. For this reason, we focus on the origins of the confirmed B-type HVSs here.

Brown (2015) argues that an origin through the Hills (1988) mechanism operating in the Galactic Centre remains the only plausible origin of the HVSs if they originate in the MW. However for HVS3, this assumption has been questioned before. Edelmann et al. (2005) noted that HVS3 is only 16.3 from the centre of the Large Magellanic Cloud (LMC) and that (neglecting the potential of the LMC and without measured proper motions) the star was consistent with being ejected from the LMC’s centre 35 Myr ago at 600 km s^{−1}. An origin in the LMC solves the problem that HVS3 would not live long enough to survive the journey from the Galactic Centre to its current location (Edelmann et al. 2005). Gualandris & Portegies Zwart (2007) found that the ejection of this star from the LMC at such a rapid velocity would require the Hills (1988) mechanism to be operating, and that the required black hole would need to be at least 10^3 M_⊙. Brown et al. (2010) used proper motions measured with the *Hubble Space Telescope* (HST) to argue that the star likely originated in the MW. However, with additional HST data,

* E-mail: d.erkal@surrey.ac.uk

Brown et al. (2015) found that HVS3 could have come from either the MW or the LMC. Perets (2009) suggests that the discrepancy between the flight time from the Galactic Centre and the stellar lifetime may be resolved by assuming that the star was ejected as a binary with hypervelocity and later merged with its companion due to internal processes. However, the ejection of hypervelocity binaries following the disruption of a stellar triple is extremely unlikely (Fragione & Gualandris 2018).

An origin in the LMC has recently been proposed for many of the other B HVSs. Boubert & Evans (2016) showed if there is a massive black hole in the LMC, then the Hills mechanism would cause stars to be ejected from the LMC, and that those stars would match the kinematic pattern of the observed HVSs. Boubert et al. (2017) investigated the ejection of stars from the LMC by the supernova of their companion and showed that this more standard scenario could also explain many of the HVSs observed in the halo.

The European Space Agency's *Gaia Space Telescope* was launched in 2013 and on the 2018 April 25 delivered its second data release (*Gaia* DR2; Gaia Collaboration et al. 2016, 2018) containing astrometry and photometry for 1692 919 135 sources, based on the first 22 months of operation. This catalogue has parallaxes and proper motions for 1331 909 727 sources, including for a majority of the HVSs considered in this work.

It is in this context that we investigate whether the B HVSs are more consistent with a MW or LMC origin, using a set of proper motions synthesized from the literature (most notably, Brown et al. 2015 obtained HVS proper motions for HVS1–HVS13) and from the newly released *Gaia* DR2 (see Table A1). In Section 2.1, we describe how we follow back in time the trajectories of the HVSs accounting for the Galactic and LMC potentials and the measurement errors. Section 3 discusses HVS3 in some detail, building the case that it has been ejected by a supermassive black hole at the centre of the LMC. In Section 4, we validate our method using mock data from the Boubert & Evans (2016) simulations of stars ejected from the LMC's centre.

2 POPULATION OF HYPERVELOCITY STARS

2.1 Method

In order to determine the origin of the HVSs, we rewind them in the combined presence of the gravitational field of the MW and the LMC. For the MW, we consider two potentials. First, we use *MWPotential2014* from Bovy (2015) that satisfies a number of observed constraints. This potential consists of a Navarro–Frenk–White (NFW) dark matter halo (Navarro, Frenk & White 1997), a Miyamoto–Nagai disc (Miyamoto & Nagai 1975), and a power-law bulge with an exponential cut-off. When using this potential, we use an offset of $(U_{\odot}, V_{\odot}, W_{\odot}) = (11.1, 24, 7.3)$ km s^{−1} from Schönrich, Binney & Dehnen (2010) and Bovy et al. (2012) for the Sun's motion relative to the local circular velocity. We assume that the Sun is located at a distance of 8.3 ± 0.1 kpc from the Galactic Centre. The second potential that we consider is the recent MW model in McMillan (2017).

For the LMC, we choose a mass of $1.5 \times 10^{11} M_{\odot}$. This is based on the several lines of reasoning that have suggested that the LMC has a mass on the order of $10^{11} M_{\odot}$ based on abundance matching (Behroozi, Wechsler & Conroy 2013; Moster, Naab & White 2013), requiring that the Small Magellanic Cloud (SMC) is bound to the LMC (Kallivayalil et al. 2013), the plethora of dwarfs around the LMC (Jethwa, Erkal & Belokurov 2016), as well as accounting for the effect of the LMC on the timing argument between

MW and M31 (Peñarrubia et al. 2016). The LMC is modelled as a Hernquist profile with a scale radius of 17.14 kpc. This profile satisfies the rotation curve measurements by van der Marel & Kallivayalil (2014). We note that we have performed the analysis with an LMC mass of $2 \times 10^{10} M_{\odot}$ and we find similar results. We use an LMC distance of 49.97 ± 1.126 kpc (Pietrzyński et al. 2013), an LMC radial velocity of 262.2 ± 0.3 km s^{−1} (van der Marel et al. 2002), and proper motions of $(\mu_{\alpha} \cos \delta, \mu_{\delta}) = (1.91 \pm 0.02, 0.229 \pm 0.047)$ mas yr^{−1} (Kallivayalil et al. 2013). We include dynamical friction from the MW on the LMC using the prescription of Hashimoto, Funato & Makino (2003).

2.2 General properties of the population

The properties of the HVSs are given in Appendix A and come from a variety of sources. *Gaia* DR2 has significantly improved the proper motions of many of the HVSs. With the updated proper motions in hand, we now integrate their orbits backwards in the MW potential to determine the point of closest approach of the HVSs and the MW. We choose to rewind the HVSs for 500 Myr that is significantly longer than their main-sequence lifetimes; most of the stars are late B or early A type with the sole exception of HVS2 (also known as US 708) that is a nearby sdO star with an evolutionary lifetime of 100 Myr (Hirsch et al. 2005). The rewinding is done by performing a Monte Carlo sampling of the 6D phase-space coordinates of the HVS based on the observational uncertainties in distance, proper motion (accounting for the covariance in proper motions from *Gaia* DR2), and radial velocity. We also sample the distance of the Sun from the Galactic Centre and the 6D phase-space coordinates of the LMC. For each realization of these quantities, we rewind each HVS for 500 Myr and determine its point of closest approach with the MW and the LMC. We then record the distance, relative velocity, and lookback time to this close passage. In addition, we determine the location where each HVS passes through the plane of the MW disc and the plane of the LMC disc (as measured in van der Marel & Kallivayalil 2014).

In the left-hand panel of Fig. 1, we show the minimum approach distance to the MW and LMC for the HVSs in the sample. Points on the top left of this figure have a closer approach to the MW than the LMC and vice versa for the points on the bottom right. The right-hand panel shows the probability of passing within 5 kpc of the centre of the MW versus the same quantity for the LMC. Several points stand out clearly in the figures. First, HVS3 is the lone outlier as clearly preferring an LMC origin. Secondly, some of the candidates, such as HVS5, LAMOST-HVS1 to LAMOST-HVS3, are much more consistent with a Galactic origin. Thirdly, the bulk of the population has a closer minimum approach to the MW rather than the LMC, though here caution is warranted as the error bars remain large and there may be systematic uncertainties in the simulations.

3 HVS3

In Fig. 1, HVS3 lies apart from the bulk of the population and appears to pass very close to the centre of the LMC. In order to investigate it further, we sample its parameters (along with the LMC's parameters) 100 000 times and consider the resulting orbits. The panels of Fig. 2 show the results from these simulations. In the left-hand panel, we show contours of the time of closest approach to the LMC and the relative velocity during this closest approach. The ejection velocity is 870^{+69}_{-66} km s^{−1}. The ejection time is $21.1^{+6.1}_{-4.6}$ Myr (median with 1σ errors). We found that these

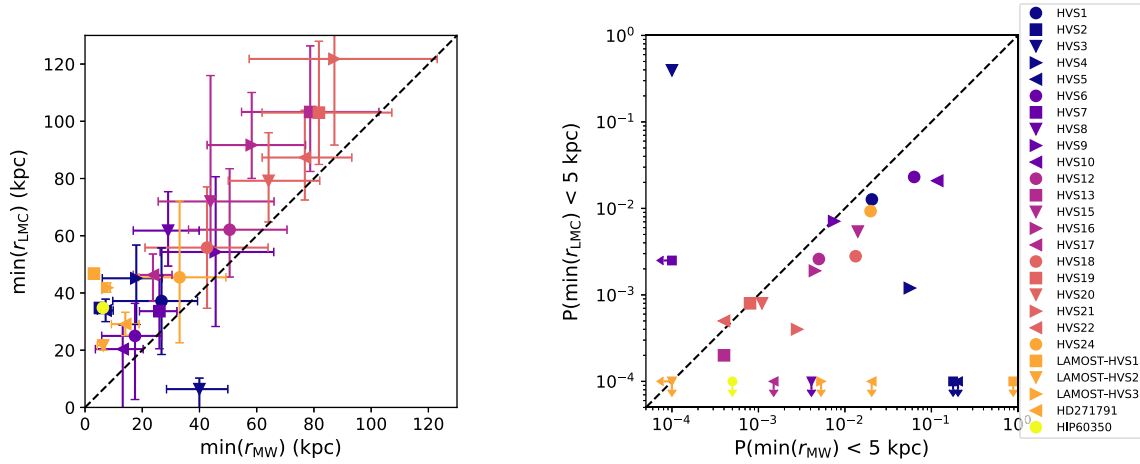


Figure 1. Left: minimum approach distance to the Milky Way (MW) and the LMC for the 26 HVSs in our sample. HVS3 stands out as being far more likely to have originated near the LMC than near the MW. Right: probability of passing within 5 kpc of the MW and the LMC over the past 500 Myr. Again, HVS3 clearly stands out as being significantly more likely to originate from near the centre of the LMC ($p = 0.40$) than the MW ($p = 10^{-4}$).

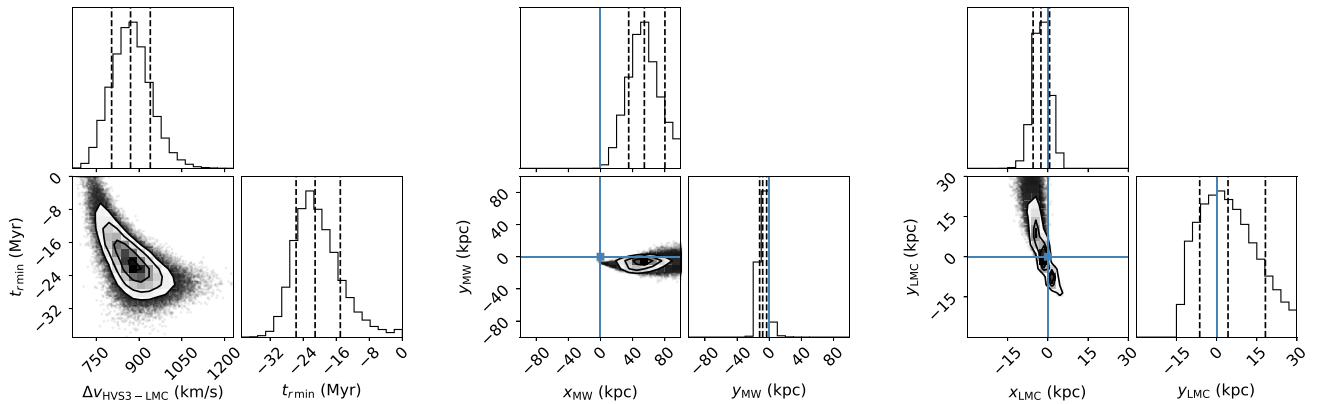


Figure 2. Left: distribution of relative velocities to the LMC and ejection times for HVS3. The dashed lines show the 15.9, 50, and 84.1 percentiles of each 1D distribution. The contours shown are 0.5σ , 1σ , 1.5σ , and 2σ . The ejection velocity is 870^{+69}_{-66} km s $^{-1}$. The ejection time is $21.1^{+6.1}_{-4.6}$ Myr (median with 1σ errors). Middle: location where HVS3 passes through the plane of the MW disc. The centre of the MW excluded at the 3σ level. The centre of the MW is a clear outlier. Right: location where HVS3 passes through the plane of the LMC disc as defined in van der Marel & Kallivayalil (2014). The centre of the LMC is just within the 1σ contour. We note that 8 per cent of the orbits for HVS3 do not pass through the plane of the LMC’s disc.

properties were quite insensitive to the mass of the LMC; using a $2 \times 10^{10} M_{\odot}$ LMC (with a scale radius of 0.74 kpc to satisfy the rotation curve measurement from van der Marel & Kallivayalil 2014) changed them by ~ 0.5 per cent. Since the LMC disc is rotating, we can also determine the ejection velocity relative to the disc. Taking the circular velocity from (van der Marel & Kallivayalil 2014) slightly increases the ejection velocity to ~ 888 km s $^{-1}$, which is well within its 1σ uncertainty and thus will not affect our result or interpretation.

The middle panel of Fig. 1 shows the locations where HVS3 passes through the Galactic plane. Note that the Galactic Centre is excluded at the 3σ level. We find that the flight time to the point of closest approach with the MW occurs $66^{+4.1}_{-4.5}$ Myr ago, significantly exceeding the main-sequence lifetime of 35 Myr for HVS3. Furthermore, this point of closest approach lies at a distance of 40^{+11}_{-10} kpc from the MW centre. The right-hand panel of Fig. 2 shows where the orbits of HVS3 pass through the plane of the LMC disc (as defined in van der Marel & Kallivayalil 2014). This shows that HVS3 is consistent with being ejected from the very centre of the LMC. This result was pre-figured in the work of Edelmann et al.

(2005) and Gualandris & Portegies Zwart (2007), but the *Gaia* DR2 proper motions have made the proposition unanswerable.

3.1 Varying the Milky Way potential

So far, we have assumed a single potential for the MW, namely that of `MWPotential2014` from Bovy (2015). In order to explore the effect of uncertainties in the MW potential on the orbit of HVS3, we consider the fits to the MW potential given in McMillan (2017). In addition to sampling the phase-space coordinates of HVS3 and the LMC, we also sample the potential parameters fit in McMillan (2017). These are the thin and thick disc surface density and scale radius, the bulge density, the NFW halo density and scale radius, and the solar position. These are sampled accounted for the correlation matrix given in McMillan (2017). The forces are implemented using `galpot` (Dehnen & Binney 1998). Finally, we also sample the Sun’s motion relative to the local standard of rest (LSR) from the values given in McMillan (2017). This improved sampling thus represents a marginalization the uncertainties in the MW potential, the Sun’s location, and the Sun’s velocity relative to the LSR. For

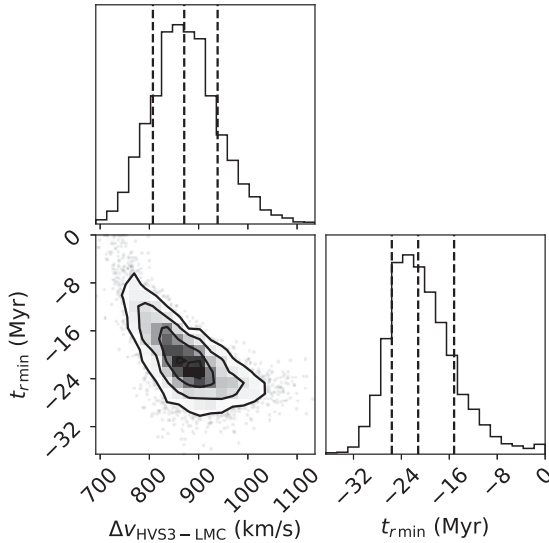


Figure 3. Distribution of relative velocities to the LMC and ejection times for HVS3 evolved in the MW potential from McMillan (2017), marginalized over the potential uncertainties. The dashed lines show the 15.9, 50, and 84.1 percentiles of each 1D distribution. The ejection velocity is 871^{+68}_{-64} km s⁻¹. The ejection time is $21.2^{+6.0}_{-4.4}$ Myr (median with 1σ errors). The similarity of this result and that in Fig. 2 shows that the orbit of HVS3 is robust.

HVS3, this produces a very similar result to what we found with the original potential. Fig. 3 shows relative velocity and ejection time for HVS3 with respect to the LMC, which looks very similar to the left-hand panel of Fig. 2 with an almost identical median and 1σ spread of the relative velocity and ejection time. The similarity of the spread suggests that the majority of the uncertainty comes from the uncertainty in the position and velocity of HVS3 and the LMC. We tested this by fixing the properties of HVS3 and the LMC, only varying the potential and solar parameters from McMillan (2017). This gives a spread of merely ~ 0.1 km s⁻¹ and < 0.1 Myr in the ejection velocity and ejection time, respectively, showing that the potential has a negligible effect.

Since the LMC is believed to have a mass on the order of $\sim 10^{11} M_{\odot}$, it is possible that the reflex motion of the MW (e.g. Gómez et al. 2015) could have an effect on the origin of the HVSs. In order to test this, we treat the MW as a particle sourcing a potential, MWPotential2014 from Bovy (2015). The rewinding procedure then integrates the orbit of the MW, the LMC, and each HVS. This had a negligible effect on their trajectories and points of closest approach (changing the ejection velocity and time by 0.4 km s⁻¹ and 0.2 Myr, respectively), likely due to the relatively short flight times for each HVS compared to the orbital time-scale of the LMC.

3.2 Origin of HVS3

The previous analysis strongly argues in favour of an origin in the LMC, as originally suggested by Edelmann et al. (2005). The inferred relative velocity of ~ 870 km s⁻¹ can be used to constrain the ejection mechanism. Gualandris, Portegies Zwart & Sipior (2005) use population synthesis of $(8+8) M_{\odot}$ binaries to show that the maximum escape velocity produced by binary evolution and supernova explosions is $\lesssim 100$ km s⁻¹, even accounting for natal kicks. Tauris (2015) investigated disrupted binaries with early, massive B-star companions ($10 M_{\odot}$) and find a maximum ejection velocity

of ~ 320 km s⁻¹. It is also extremely unlikely that HVS3 is a binary system ejected as a result of a large asymmetric supernova kick, as the binary would have been unbound by the explosion.

The large observed velocity therefore suggests an origin in a dynamical encounter in the LMC. Encounters with main-sequence stars, neutron stars, or stellar mass black holes eject stars with maximum velocities of the order of the binary orbital velocity (e.g. Gualandris et al. 2005). Two-body gravitational encounters between single stars, and gravitational interactions between stars and binaries in dense, compact clusters or cluster cores cannot explain the measured velocity of HVS3 (e.g. Yu & Tremaine 2003; Perets & Šubr 2012). Only a Hills-type encounter with a massive black hole is able to produce a recoil velocity consistent with observations. In this case the ejection velocity is given by (Hills 1988; Bromley et al. 2006)

$$V_{ej} \sim 640 \text{ km s}^{-1} \left(\frac{a_b}{0.2 \text{ au}} \right)^{-1/2} \left(\frac{m_1 + m_2}{16 M_{\odot}} \right)^{1/3} \left(\frac{M_{BH}}{10^3 M_{\odot}} \right)^{1/6}, \quad (1)$$

where a_b represents the binary semimajor axis, m_1 and m_2 the primary and secondary masses, and M_{BH} the mass of the massive black hole. An ejection velocity of 871^{+68}_{-64} km s⁻¹ thus requires a black hole mass of at least $4 \times 10^3 - 10^4 M_{\odot}$. This is in good agreement with the early estimate of Gualandris & Portegies Zwart (2007) based on scattering experiments.

A black hole of this mass, a so-called intermediate-mass black hole (IMBH) could be found either at the centre of the LMC or in a star cluster. The first case would help us better understand how black holes form in dwarf galaxies given the recent detections in other dwarfs (e.g. Filippenko & Ho 2003; Valluri et al. 2005; Reines et al. 2011). In the latter case, the IMBH could have been formed by runaway collisions (Zwart et al. 2004). Two clusters have been suggested by Gualandris & Portegies Zwart (2007) as possible birthplaces of HVS3, NGC 2004, and NGC 2100, both having a large central concentration and ages consistent with the travel time of HVS3. A large concentration is required to ensure mass segregation of the massive stars to the cluster core in a few Myr and to trigger a sequence of collisions to form the very massive star that eventually collapses to form the IMBH. Gualandris & Portegies Zwart (2007) estimate an ejection rate of 5×10^{-7} yr⁻¹ for a typical cluster with central density of 2×10^4 pc⁻³ and stellar velocity dispersion of 10 km s⁻¹. Such a rate is consistent with the observation of HVS3, however we caution that the estimate of the theoretical rate relies on specific assumptions regarding e.g. the stellar mass function and the binary semimajor axis distribution. We further note that Gualandris & Portegies Zwart (2007) assume direct collapse of the massive star to an IMBH without mass loss, and this is likely unrealistic (Petts & Gualandris 2017). Finally, we note that NGC 2004 and NGC 2100 are both located within the 2σ contour in the right-hand panel of Fig. 2 and have radial velocities similar to the LMC (Martayan et al. 2006; Patrick et al. 2016), which shows they are also dynamically consistent with being the origin of HVS3. In light of current uncertainties in theoretical models and difficulties in detecting IMBHs in star cluster, the detection of HVS3 is particularly noteworthy.

4 TESTING WITH MOCK SIMULATIONS

In this section we will use two N -body simulations with HVSs ejected from the MW and LMC centres to test how well we can

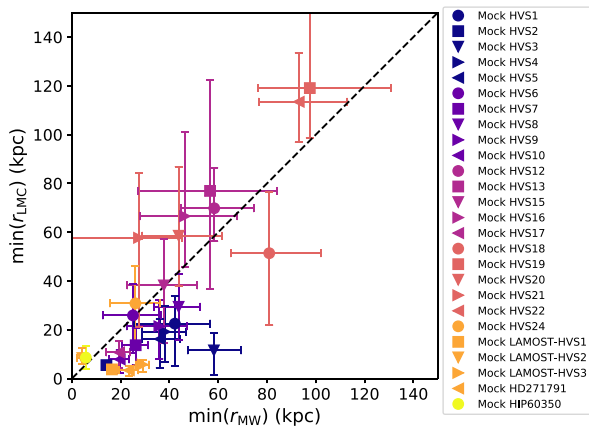


Figure 4. Minimum approach distance to the MW and the LMC for a mock sample of hypervelocity stars (HVSs) that were ejected by a massive black hole in the centre of the LMC.

recover their properties, as well as estimate the probability of misclassifying a star.

The simulations used in this work are described in Boubert et al. (2017). These consist of N -body simulations evolved with a modified version of GADGET-3, which is an improved version of GADGET-2 (Springel 2005). The code has been modified so that we can track the centre of either the MW or the LMC on the fly. It has also been modified to eject massless tracer particles (representing HVSs) from the centre of either galaxy.

The simulations (see Boubert et al. 2017, for more details) evolve an N -body MW (bulge, disc, and halo) and an N -body LMC (disc and halo) that are initialized so that the LMC ends up within 2σ of its observed location and velocity at the end of the simulation. We discuss two separate simulations below, one where HVSs are ejected from the centre of the LMC and one where they are ejected from the MW centre.

4.1 Tests with stars ejected from the LMC

In this section, we take a mock sample of HVSs from Boubert et al. (2017) that were ejected by a massive black hole in the centre of the LMC. These were ejected with a velocity distribution governed by the Hills mechanism, assuming a black hole mass of $1.7 \times 10^5 M_\odot$ in the centre of the LMC (see Boubert & Evans 2016, for more details). The simulation was evolved for 350 Myr that is sufficient to model the young stars ejected from the LMC.

For each HVS in our sample, we locate the closest particle to the 3D location of the HVS (ignoring distance uncertainties). This gives us a sample of 26 mock HVSs that were ejected from the LMC and are close to the observed HVSs. We note that almost all of the observed HVSs had analogues within 5 kpc of their present day position. The distance, proper motion, and radial velocity of each mock star are then perturbed by the observational errors of its associated HVS. For each of these mock HVSs, we then repeat the same rewinding procedure described in Section 2 to determine how well we can identify the origin of these stars. We note that the rewinding procedure was identical to what we did on the observed sample of HVSs, except we changed the mass of the MW’s NFW to be $10^{12} M_\odot$, equal to the simulated MW’s halo mass.

Fig. 4 shows the distance of closest approach to the MW and the LMC for this mock sample. While many of the mock HVSs are consistent with coming from the LMC (i.e. the clustering of

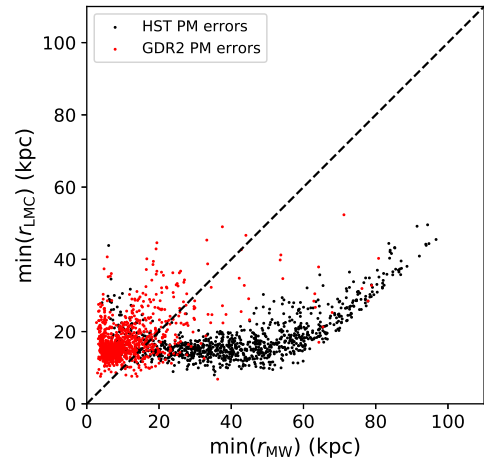


Figure 5. Comparison of minimum approach distance to the MW and LMC for 1000 mock stars ejected from the MW chosen at the location of HVS3. We see that with *HST* proper motions, many of the mocks appear to have passed closer to the MW than the LMC. However, this is a bias due to the large errors with *HST*. With *Gaia* DR2 (GDR2) errors, almost all of the stars are correctly inferred to pass much closer to the MW than the LMC. Thus, the proper motion quality of GDR2 is critical to correctly determine whether HVS3 originated in the MW or the LMC.

stars near the x -axis of the figure), there are many stars that appear inconsistent with an LMC origin. Many of the stars are distant from both the MW and the LMC (similar to the observed HVSs, left-hand panel of Fig. 1). This suggests that there is a significant possibility that other stars in this sample of 26 could have originated in the LMC. Improved data are needed to determine their origin. However, this figure is clearly different from the left-hand panel of Fig. 1 that shows that only one of the observed HVSs comes from the LMC. Thus, it appears that the majority of the observed sample did not come from the LMC.

4.2 Testing HVS3 with stars ejected from the Milky Way

Next, we take mock stars from simulations that include a population of HVSs ejected from the MW centre. We use this simulation to assess how often we misclassify a HVS ejected from the MW as coming from the LMC. These simulations are almost identical to the ones described in the previous section except the HVSs are ejected from the MW centre instead of from the LMC. The stars are ejected with a velocity distribution similar to that in Boubert et al. (2017) except with a black hole mass of $4 \times 10^6 M_\odot$ (Ghez et al. 2005). The simulation was evolved for 1 Gyr.

We create a mock sample by sampling from the distance to HVS3 and then selecting the closest star in the simulation (in the direction towards HVS3) that has not already been selected. This gives us a sample of 1000 mock stars drawn from a similar location to HVS3. We note that we do not make any selection on the velocities of the particles in the simulation.

Each particle is then assigned the observational errors of HVS3 (in distance, proper motions, and radial velocity) and a mock observation is performed, perturbing the particles properties from their true values. These values represent the mock star’s properties and we sample from its errors as in Section 2. For this procedure, we consider two sets of errors for the proper motion: *HST* errors from Brown et al. (2015) and the proper motion errors from *Gaia* DR2. This comparison is instructive since it allows us to see the resolving power of *Gaia*.

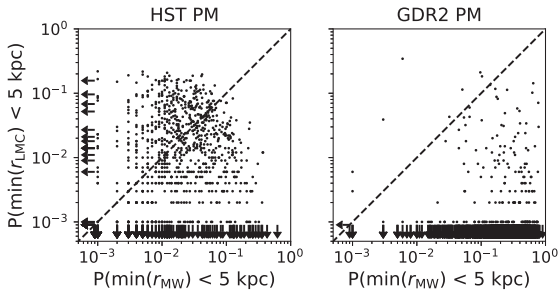


Figure 6. Comparison of the probability of approaching within 5 kpc for 1000 mock stars ejected from the MW selected at the location of HVS3. This figure shows that the false positive rate of misclassifying a MW HVS as coming from the LMC is approximately one in 1000.

Fig. 5 shows the closest approach distance to the MW and the LMC for the sample of mock stars. With *HST* quality proper motions (based on the uncertainties for HVS3 in Brown et al. 2015), there is a significant risk of misclassifying a MW HVS as coming from the LMC. This bias is due to the fact that HVS3 is closer to the LMC than the MW and thus there is a larger spread in the orbits by the time they reach the MW. However, if we use the proper motions from *Gaia* DR2, we find a significant improvement with few MW HVS appearing to originate in the LMC. Fig. 6 shows the probability of these mock HVSS passing within 5 kpc of either the MW of the LMC. This shows that *Gaia* DR2 quality observations were needed to reduce the risk of misclassifying a MW HVS as coming from the LMC. Based on this figure we estimate that the chance that HVS3 is misclassified is approximately one in 1000.

5 CONCLUSION

We present a first look at the orbits of 26 HVSS around the MW using proper motions from the recent *Gaia* DR2. These exquisite proper motions allow us to determine the origin of a number of these HVSS. While many of them appear to come from the MW, HVS3 is a clear outlier and comes from the LMC, thus confirming the original suggestions of Edelmann et al. (2005) and Gualandris & Portegies Zwart (2007). We find that HVS3 had a closest approach with respect to the LMC $21.1^{+6.1}_{-4.6}$ Myr ago, with a relative velocity of 870^{+69}_{-66} km s⁻¹, and is consistent with being ejected from the very centre of the LMC. This high ejection velocity rules out all scenarios except for the Hills mechanism, requiring a black hole mass of at least 4×10^3 – 10^4 M_⊙. This provides strong evidence that the LMC harbours a massive black hole.

We run a number of tests to ensure that this result is robust. We have marginalized over the MW potential from McMillan (2017), which has a negligible effect on our results. We also run our analysis on two *N*-body simulations that contain HVSS from the LMC and the MW. The first test with mock HVSS from the LMC showed that if all of the 26 HVSS in our sample originated from the LMC, we should have found more HVSS with a close LMC passage. This tentatively suggests that at least some of the 26 HVS did not originate in the LMC. Interestingly, this test also revealed that a number of the poorly constrained HVSS are consistent with an LMC origin. The second test with a mock of MW HVSS was only performed for HVS3. This showed that *Gaia* DR2 quality proper motions were needed to confirm whether HVS3 indeed originated in the LMC, and thus to provide strong evidence of a massive black hole near the LMC's centre.

ACKNOWLEDGEMENTS

DB thanks the UK Science and Technology Facilities Council for supporting his PhD. This work has made use of data from the European Space Agency (ESA) mission *Gaia* (<https://www.cosmos.esa.int/gaia>), processed by the *Gaia* Data Processing and Analysis Consortium (DPAC, <https://www.cosmos.esa.int/web/gaia/dpac/consortium>). Funding for the DPAC has been provided by national institutions, in particular the institutions participating in the *Gaia* Multilateral Agreement. FA acknowledges support from an E. Rutherford fellowship (ST/P00492X/1) from the Science and Technology Facilities Council. We thank the anonymous referee whose comments improved the clarity of this work.

REFERENCES

- Behroozi P. S., Wechsler R. H., Conroy C., 2013, *ApJ*, 770, 57
 Bonanos A. Z., López-Morales M., Hunter I., Ryans R. S. I., 2008, *ApJ*, 675, L77
 Boubert D., Evans N. W., 2016, *ApJ*, 825, L6
 Boubert D., Erkal D., Evans N. W., Izzard R. G., 2017, *MNRAS*, 469, 2151
 Boubert D., Guillochon J., Hawkins K., Ginsburg I., Evans N., 2018, *MNRAS*, 479, 2789
 Bovy J., 2015, *ApJS*, 216, 29
 Bovy J. et al., 2012, *ApJ*, 759, 131
 Bromley B. C., Kenyon S. J., Geller M. J., Barcikowski E., Brown W. R., Kurtz M. J., 2006, *ApJ*, 653, 1194
 Brown W. R., 2015, *ARA&A*, 53, 15
 Brown W. R., Geller M. J., Kenyon S. J., Kurtz M. J., 2005, *ApJ*, 622, L33
 Brown W. R., Geller M. J., Kenyon S. J., Kurtz M. J., 2006, *ApJ*, 647, 303
 Brown W. R., Geller M. J., Kenyon S. J., Kurtz M. J., Bromley B. C., 2007, *ApJ*, 671, 1708
 Brown W. R., Anderson J., Gnedin O. Y., Bond H. E., Geller M. J., Kenyon S. J., Livio M., 2010, *ApJ*, 719, L23
 Brown W. R., Geller M. J., Kenyon S. J., 2014, *ApJ*, 787, 89
 Brown W. R., Anderson J., Gnedin O. Y., Bond H. E., Geller M. J., Kenyon S. J., 2015, *ApJ*, 804, 49
 Dehnen W., Binney J., 1998, *MNRAS*, 294, 429
 Edelmann H., Napiwotzki R., Heber U., Christlieb N., Reimers D., 2005, *ApJ*, 634, L181
 Filippenko A. V., Ho L. C., 2003, *ApJ*, 588, L13
 Fragione G., Gualandris A., 2018, *MNRAS*, 475, 4986
 Gaia Collaboration et al., 2016, *A&A*, 595, A1
 Gaia Collaboration et al., 2018, *A&A*, 616, A1
 Geier S. et al., 2015, *Science*, 347, 1126
 Ghez A. M., Salim S., Hornstein S. D., Tanner A., Lu J. R., Morris M., Becklin E. E., Duchêne G., 2005, *ApJ*, 620, 744
 Gómez F. A., Besla G., Carpintero D. D., Villalobos Á., O'Shea B. W., Bell E. F., 2015, *ApJ*, 802, 128
 Gualandris A., Portegies Zwart S., 2007, *MNRAS*, 376, L29
 Gualandris A., Portegies Zwart S., Sipior M. S., 2005, *MNRAS*, 363, 223
 Hashimoto Y., Funato Y., Makino J., 2003, *ApJ*, 582, 196
 Heber U., Edelmann H., Napiwotzki R., Altmann M., Scholz R.-D., 2008a, *A&A*, 483, L21
 Heber U., Hirsch H. A., Edelmann H., Napiwotzki R., O'Toole S. J., Brown W., Altmann M., 2008b, in Heber U., Jeffery C. S., Napiwotzki R., eds, ASP Conf. Ser. Vol. 392, Hot Subdwarf Stars and Related Objects. Astron. Soc. Pac., San Francisco, p. 167
 Hills J. G., 1988, *Nature*, 331, 687
 Hirsch H. A., Heber U., O'Toole S. J., Bresolin F., 2005, *A&A*, 444, L61
 Huang Y. et al., 2017, *ApJ*, 847, L9
 Irrgang A., Przybilla N., Heber U., Nieva M. F., Schuh S., 2010, *ApJ*, 711, 138
 Jethwa P., Erkal D., Belokurov V., 2016, *MNRAS*, 461, 2212
 Kallivayalil N., van der Marel R. P., Besla G., Anderson J., Alcock C., 2013, *ApJ*, 764, 161
 McMillan P. J., 2017, *MNRAS*, 465, 76

Martayan C., Frémat Y., Hubert A.-M., Floquet M., Zorec J., Neiner C., 2006, *A&A*, 452, 273
Miyamoto M., Nagai R., 1975, *PASJ*, 27, 533
Moster B. P., Naab T., White S. D. M., 2013, *MNRAS*, 428, 3121
Navarro J. F., Frenk C. S., White S. D. M., 1997, *ApJ*, 490, 493
Patrick L. R., Evans C. J., Davies B., Kudritzki R.-P., Hénault-Brunet V., Bastian N., Lapenna E., Bergemann M., 2016, *MNRAS*, 458, 3968
Peñarrubia J., Gómez F. A., Besla G., Erkal D., Ma Y.-Z., 2016, *MNRAS*, 456, L54
Perets H. B., 2009, *ApJ*, 690, 795
Perets H. B., Šubr L., 2012, *ApJ*, 751, 133
Petts J. A., Gualandris A., 2017, *MNRAS*, 467, 3775
Pietrzyński G. et al., 2013, *Nature*, 495, 76
Przybilla N., Nieva M. F., Heber U., Firnstein M., Butler K., Napiwotzki R., Edelmann H., 2008, *A&A*, 480, L37
Reines A. E., Sivakoff G. R., Johnson K. E., Brogan C. L., 2011, *Nature*, 470, 66

Schönrich R., Binney J., Dehnen W., 2010, *MNRAS*, 403, 1829
Springel V., 2005, *MNRAS*, 364, 1105
Tauris T. M., 2015, *MNRAS*, 448, L6
Valluri M., Ferrarese L., Merritt D., Joseph C. L., 2005, *ApJ*, 628, 137
van der Marel R. P., Kallivayalil N., 2014, *ApJ*, 781, 121
van der Marel R. P., Alves D. R., Hardy E., Suntzeff N. B., 2002, *AJ*, 124, 2639
Yu Q., Tremaine S., 2003, *ApJ*, 599, 1129
Zheng Z. et al., 2014, *ApJ*, 785, L23
Zwart S. F. P., Baumgardt H., Hut P., Makino J., McMillan S. L. W., 2004, *Nature*, 428, 724

APPENDIX A: PROPERTIES OF HVS

We list the properties of the 26 HVSs studied in this work in Table A1.

Table A1. The 26 hypervelocity stars (HVSs) considered in this work. Almost all of the proper motion measurements are from *Gaia* DR2 except for HVS1, HVS4, HVS13, and HIP 60350.

ID	RA	Dec.	$\mu_\alpha \cos \delta$ (mas yr ⁻¹)	μ_δ (mas yr ⁻¹)	Corr($\mu_\alpha \cos \delta, \mu_\delta$)	v_{hel} (km s ⁻¹)	D_{hel} (kpc)	Ref.
HVS1	09:07:44.99	+02:45:06.9	0.1 ± 0.3	−0.1 ± 0.2	...	831.1 ± 5.7	107 ± 15	1
HVS2	09:33:20.86	+44:17:05.4	−5.363 ± 0.391	1.285 ± 0.382	−0.2092	917 ± 7	8.5 ± 1	1, 2, 3
HVS3	04:38:12.8	−54:33:12	0.851 ± 0.110	1.936 ± 0.162	0.1899	723 ± 3	61 ± 10	1, 2
HVS4	09:13:01.01	+30:51:19.8	−0.2 ± 0.4	−0.4 ± 0.4	...	600.9 ± 6.2	64 ± 9.8	1
HVS5	09:17:59.48	+67:22:38.3	−0.023 ± 0.176	−1.179 ± 0.268	0.2162	545.5 ± 4.3	45 ± 5.2	1, 2
HVS6	11:05:57.45	+09:34:39.47	−0.378 ± 0.664	−0.503 ± 0.507	−0.0242	609.4 ± 6.8	55 ± 6.9	1, 2
HVS7	11:33:12.12	+01:08:24.9	−0.677 ± 0.373	0.457 ± 0.253	−0.2767	526.9 ± 3	52 ± 6.4	1, 2
HVS8	09:42:14.04	+20:03:22.1	−0.972 ± 0.365	0.117 ± 0.369	−0.3844	499.3 ± 2.9	53 ± 9.8	1, 2
HVS9	10:21:37.08	−00:52:34.8	0.412 ± 0.743	−0.213 ± 0.747	−0.2503	616.8 ± 5.1	74 ± 12	1, 2
HVS10	12:03:37.85	+18:02:50.4	−2.597 ± 1.288	−0.788 ± 0.494	0.0151	467.9 ± 5.6	52 ± 5.8	1, 2
HVS12	10:50:09.59	+03:15:50.67	0.42 ± 1.377	0.285 ± 0.993	0.2614	552.2 ± 6.6	66 ± 8.5	1, 2
HVS13	10:52:48.3	−00:01:33.94	−0.9 ± 0.4	0.5 ± 0.4	...	569.3 ± 6.1	105 ± 19	1
HVS15	11:33:41.09	−01:21:14.25	−0.498 ± 1.291	−0.487 ± 0.567	−0.0546	461 ± 6.3	67 ± 10	2, 4
HVS16	12:25:23.4	+05:22:33.84	−1.895 ± 1.518	−1.145 ± 0.856	−0.429	429.8 ± 7	71 ± 12	2, 4
HVS17	16:41:56.39	+47:23:46.12	−1.034 ± 0.198	−1.065 ± 0.323	0.0801	250.2 ± 2.9	49 ± 4	2, 4
HVS18	23:29:04.94	+33:00:11.47	−0.123 ± 0.656	−0.119 ± 0.495	0.213	237.3 ± 6.4	80 ± 11	2, 4
HVS19	11:35:17.75	+08:02:01.49	−0.295 ± 1.790	0.413 ± 1.224	−0.3625	592.8 ± 11.8	98 ± 15	2, 4
HVS20	11:36:37.13	+03:31:06.84	0.453 ± 1.451	0.569 ± 1.014	−0.2955	512.1 ± 8.5	76 ± 11	2, 4
HVS21	10:34:18.25	+48:11:34.57	0.099 ± 0.693	−0.263 ± 0.881	−0.3749	356.8 ± 7.5	113 ± 21	2, 4
HVS22	11:41:46.44	+04:42:17.29	0.184 ± 2.024	1.987 ± 1.443	−0.2758	597.8 ± 13.4	85 ± 13	2, 4
HVS24	11:11:36.44	+00:58:56.44	0.301 ± 0.777	−0.408 ± 0.578	−0.1616	492.5 ± 5.3	56 ± 7	2, 4
LAMOST-HVS1	09:12:06.52	+09:16:21.8	−3.537 ± 0.110	−0.62 ± 0.093	−0.2516	611.65 ± 4.63	13.91 ± 2	2, 5
LAMOST-HVS2	16:20:20.77	+37:47:39.9	−2.563 ± 0.056	−0.924 ± 0.072	0.2943	341.1 ± 7.79	22.24 ± 4.6	2, 6
LAMOST-HVS3	03:21:17.08	+19:07:36.2	1.509 ± 0.199	−0.281 ± 0.155	0.0972	361.38 ± 12.52	22.32 ± 2.5	2, 6
HD 271791	06:02:27.88	−66:47:28.68	−0.619 ± 0.067	4.731 ± 0.071	0.0996	441 ± 1	21 ± 4	2, 7
HIP 60350	12:24:30.23	+34:57:58.72	−13.51 ± 1.31	16.34 ± 1.37	...	262 ± 5	3.1 ± 0.6	8

Note. References: 1 – Brown et al. (2015); 2 – Gaia Collaboration et al. (2018); 3 – Geier et al. (2015); 4 – Brown et al. (2014); 5 – Zheng et al. (2014); 6 – Huang et al. (2017); 7 – Heber et al. (2008b); 8 – Irrgang et al. (2010).

This paper has been typeset from a \LaTeX file prepared by the author.